

Carrier-envelope phase-controlled laser-surface interactions

Péter Dombi and Péter Rácz

Research Institute for Solid-State Physics and Optics,
H-1121 Budapest, Konkoly-Thege M. út 29-33, Hungary / E-mail: dombi@szfki.hu

ABSTRACT

Carrier-envelope phase-stabilized laser pulses brought significant advances in investigating laser-solid interactions, as well, with the potential of revealing carrier dynamics in solids on unprecedented time-scales. More specifically, multiphoton induced photoemission from metals proved to be sensitive to the waveform of few-cycle pulses, however, underlying mechanisms are not fully understood. Combining surface plasmonic effects with photoemission demonstrates a potentially more promising approach to investigate laser-surface interactions induced by few-cycle pulses. Numerical results from a simple model on this phenomenon are presented. Related to this, previously unaddressed carrier-envelope phase phenomena in the vicinity of the focus are also considered.

Keywords: ultrafast phenomena, surface plasmons, multiphoton processes, few-cycle pulses, carrier-envelope phase

1. INTRODUCTION

Optical waveform control of recollision processes of atomic electrons has brought deeper insight into atomic physics since the reproducible generation of attosecond light pulses in gas targets was enabled by carrier-envelope (CE) phase control of few-cycle light pulses (see Ref. 1 and references therein). Similarly, in solids, the CE phase proved to play a decisive role in governing various charge transfer and photoemission processes, as measured with the first CE phase stabilized oscillators²⁻⁵. These experiments revealed several new aspects of the underlying light-matter interaction physics, even though many of these processes are not fully understood and there is substantial discrepancy between various semiclassical and quantum mechanical models and measured results.

Governing electron motion on atomic time-scales also prompts the question whether these processes can be simultaneously resolved on atomic spatial scales, too. As a more recent development, first pioneering coherent control experiments in nanoplasmonic systems underpin the possibility of controlling electronic motion on the nanoscale with visible laser pulses⁶. However, most methods of femtochemistry and attophysics are still waiting to be applied to nanoscale objects. As first steps in this direction, promising studies pave the way towards nanometer and attosecond resolution surface characterization schemes⁷ and existing schemes of ultrafast electron diffraction and microscopy offer a form of ultrahigh 4D resolution, too^{8,9}. For some of these methods pump-probe-like methods new, ultrafast photoelectron sources need to be applied. Therefore, testing new schemes for the production of well-behaved ultrashort electron bunches has become of central interest in many research groups¹⁰⁻¹². Carrier-envelope phase effects can play a substantial role in the operation of such novel photocathode schemes, one of which is to be scrutinized in Section 3.

Interaction of few-cycle pulses with surfaces poses more complex questions in terms of diffraction phenomena than laser-atom interactions. In most experimental schemes the surface is placed at a non-normal incidence angle into a focussed beam. This means that one has to investigate the effective carrier-envelope phase value at each point of the surface and establish whether any spatial smearing effect could reduce the CE phase sensitivity in the experiment. Section 4 deals with this issue.

2. SURFACE EXPERIMENTS WITH CARRIER-ENVELOPE PHASE-STABILIZED LASERS

The self-referencing or f -to- $2f$ technique allows control of CE phase evolution in the typically multi-MHz train of pulses by stabilizing $\Delta\phi$, the pulse-to-pulse CE phase shift in the output of a mode-locked laser¹³. Exploiting this technology laser systems were developed, delivering CE phase stabilized pulses as short as 3.7 fs¹⁴. However, an f -to- $2f$ interferometer usually used in this scheme is not suitable for measuring the absolute value of ϕ ; only the value of the pulse-to-pulse phase shift ($\Delta\phi$) can be stabilized. With such laser systems, however, basic experiments could be carried out demonstrating the effect of the optical waveform on laser-solid interactions. In this section such a standard measurement setup will be presented.

To detect photoelectron emission in the multiphoton regime (which was predicted to have the desired CE phase-sensitivity^{15,16}), we used a modified electron multiplier tube with the cathode substituted with a gold-coated nickel piece. The p-polarized, CE phase-stabilized laser beam impinged on the surface at an angle of incidence of 70°. The photocurrent from the cathode was found to exhibit a power-law scaling with intensity: I^3 , and a modulation at f_{ref} , the reference frequency to which the carrier-envelope phase evolution in the mode-locked pulse-train was locked. This modulation (which had a very small amplitude) was observed by a lock-in amplifier referenced to f_{ref} thereby providing proof of the optical waveform directly influencing the photoemission yield^{2,3}. As a further, ultimate evidence for the CE phase-sensitivity of the photocurrent, the in-phase component of the lock-in output was found to evolve quasi-periodically upon increasing the propagation length of the pulses in a pair of extracavity wedges, as shown in Fig.1. Shifting one of the wedges perpendicular to the beam means that the phase difference between the two periodic, electronic signals on the input of the lock-in also shift continuously, thereby providing the observed periodicity in the in-phase component of the lock-in output.

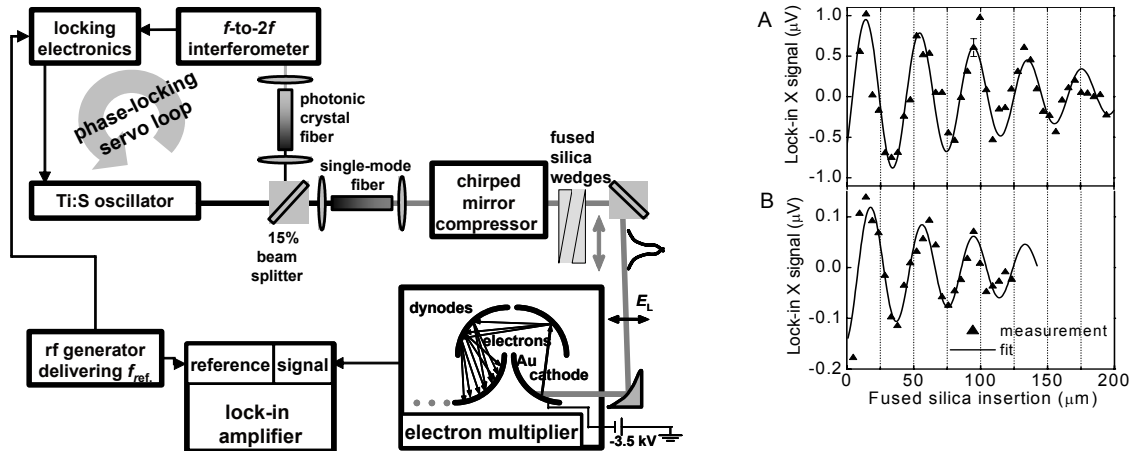


Fig. 1. Typical experimental scheme for measuring CE phase effects in laser-surface interactions also depicting the phase stabilization servo loop. Graphs A and B depict two measurement runs with two different pulse lengths. The observed oscillation in one of the components of the lock-in output signal with respect to shifting the fused silica wedge in the beam served as a proof of CE phase sensitivity of multi-photon-induced photoelectron emission.

The observed modulation depth of << 1% in the electron signal, however, prompts questions about the models used to describe this phenomenon. Both fully quantum mechanical and semiclassical calculations show that the observed effect should be much more pronounced than our previous observation, with a modulation depth of up to 30%^{15,16}. Limited experimental circumstances (such as the lack of ultrahigh vacuum conditions or the lack of using a single-crystal surface) alone can not explain such a substantial discrepancy. Therefore these experiments prompt further questions about ultrafast dynamics of these electronic transitions induced by a small number of optical cycles. There are some

suggestions on how to resolve the discrepancy^{16,17}, however, these ideas are not easy to prove experimentally, require complex experimental apparatus similar to those used in attophysics experiments and direct results are difficult to extract from such measurements.

3. ELECTRONS IN THE FIELD OF CARRIER-ENVELOPE PHASE-CONTROLLED SURFACE PLASMONS

More recently, we turned our attention to a more advanced scheme where the role of the few-cycle, infrared laser field is not simply to induce photoemission from the surface but also to govern free electron motion in a way which enables the usage of standard electron spectroscopic techniques. This phenomenon is surface plasmon (SP) enhanced electron acceleration, where the observation of the quasi-ponderomotive motion of electrons in plasmonic fields can help gaining deeper insight into the photoemission process itself, too.

SP enhanced electron acceleration is a recently discovered acceleration method in the evanescent field of surface electromagnetic waves (SPs)^{18,19}. More recent most conspicuous results include electron acceleration in SP fields up to keV energies (without external dc fields) with simple Ti:sapphire laser oscillators¹² and predictions about the carrier-envelope phase dependence of this phenomenon²⁰. The process is also interesting for the development of ultrafast methods where a well-controlled electron source is needed with high repetition rate.

We carried out numerical examinations of the relevant properties of such a source when the interacting laser pulse is composed of only few optical cycles, in addition, we consider photoelectron emission in the tunnelling regime. This is, as opposed to other simulations in this field, a much more realistic approach since inherent field enhancement effects occur upon SP coupling²².

2.1 Simulation methods

We modelled surface plasmon enhanced electron acceleration in a computationally more efficient way than previous approaches using a semiclassical a model analogous to the 3-step model of high harmonic generation²¹. SP enhanced electron acceleration involves several clearly distinct physical processes such as the coupling of the free-space and plasmonic electromagnetic fields, photoelectron emission from the metal layer and the subsequent acceleration of free electrons by the decaying plasmon field on the vacuum side of the surface. Therefore the steps of our model correspond to these individual, easily separable processes. First we gained analytic formulae for SP fields instead of the computationally intensive complete numerical solution of Maxwell's equations in the Kretschmann-Raether SP coupling configuration¹². Based on the well-known fact that SP fields decay exponentially away from the surface²² we took the expression of the SP field components on the vacuum side of the metal layer in the form of

$$E_y^{SP}(x, y, t) = \eta E_0 E_{env}(x, t) \cos(k_{SP}x - \omega_0 t + \varphi_0) \exp(-\alpha y) \quad (1a)$$

$$E_x^{SP}(x, y, t) = \eta a E_0 E_{env}(x, t) \cos\left(k_{SP}x - \omega_0 t - \frac{\pi}{2} + \varphi_0\right) \exp(-\alpha y) \quad (1b)$$

where E_0 is the field amplitude, $E_{env}(x, t)$ is an envelope function determined by the temporal and spatial beam profiles of the incoming Gaussian pulse, η is the field enhancement factor resulting from plasmon coupling²², k_{SP} is the plasmon wave number, ω_0 is the carrier frequency of the pulse, φ_0 is the carrier-envelope phase and α is the decay length of the plasmonic field in vacuum. For the accurate determination of the field we used the evanescent decay parameter $\alpha = 247 \text{ nm}^{-1}$ from previous non-approximative studies carried out for the same input parameters for laser pulses having a central wavelength of 800 nm²³. We used the value of $a = 0.3$ according to the notion that the amplitudes of the x - and y -components of the plasmonic field show this ratio according to the numerical solution of Maxwell's equations²³.

We concluded that the field given by (1a-b) approximates the exact SP field with a very good accuracy by comparing our results to those of Ref. 23. One can examine the distribution of the field amplitude in the vicinity of the surface in Fig. 2 (false colour representation) showing very good agreement with the above-mentioned calculation and we also succeeded in reproducing the vector representation of the field depicted in Fig. 3. of Ref. 23 with this method (not depicted here).

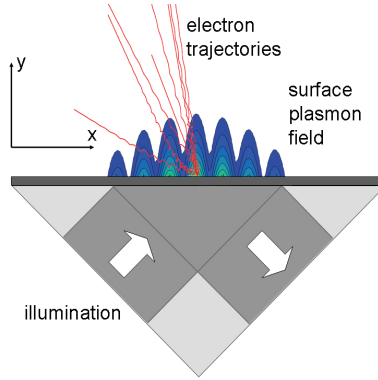


Fig. 2. Setup for the generation of electron beams by surface plasmon enhanced electron acceleration with field amplitudes and electron trajectories illustrating the model used. For further details see text.

As a second step, we placed a point array along the prism surface and examined the spatial and temporal distribution of the photoemission (induced by the plasmon field) in the tunnelling regime by applying the Fowler-Nordheim equation^{10,11}. This describes the instantaneous tunnelling current and is routinely used in studies involving electron emission from metal nanotips^{10,11}. The assumption of tunnelling emission is a more realistic starting point for such a simulation than the previously used multiphoton assumption^{12,23}. This is because experimental evidence shows efficient electron acceleration for plasmon fields of 1.8×10^9 V/cm¹² and the corresponding Keldysh-gamma of 0.01 justify the usage of tunnelling formulae. Physically, tunnelling emission sets in in this scheme even for lower driving intensities because of the inherent field enhancement phenomenon of surface plasmonic fields (with an E -field enhancement factor of 3-4 for flat and up to 100 for rough surfaces). This way we ended up with a spatially and temporally resolved map of tunnelling probabilities determined by the SP field.

Thirdly, we scrutinized vacuum electron trajectories in the plasmon field for each point in the above-mentioned array and for several emission instants. Some representatively chosen trajectories can be seen in Fig. 2 (red curves). In some cases the electron trajectories involved a recollision with the metal surface and when this happened, no electron emission was assumed. In all other cases the final kinetic energies and directions of the photoemitted and accelerated electrons were placed in a matrix for each emission point in space. This way we ended up with novel acceleration maps carrying both nanometer-scale spatial and high-resolution spectral information of the process. With these steps both microscopic and (by integrating the emission map along the spatial coordinate) macroscopic electron spectra and emission distributions can be generated. We checked that macroscopic spectra generated this way reproduce former measurement and simulation results (published in Refs. [12,23]) extremely well, including basic scaling laws, such as the linear scaling of the highest electron energy with the field intensity²³. Thereby the applicability of analytic field expressions was confirmed supporting the correctness of this simplified model.

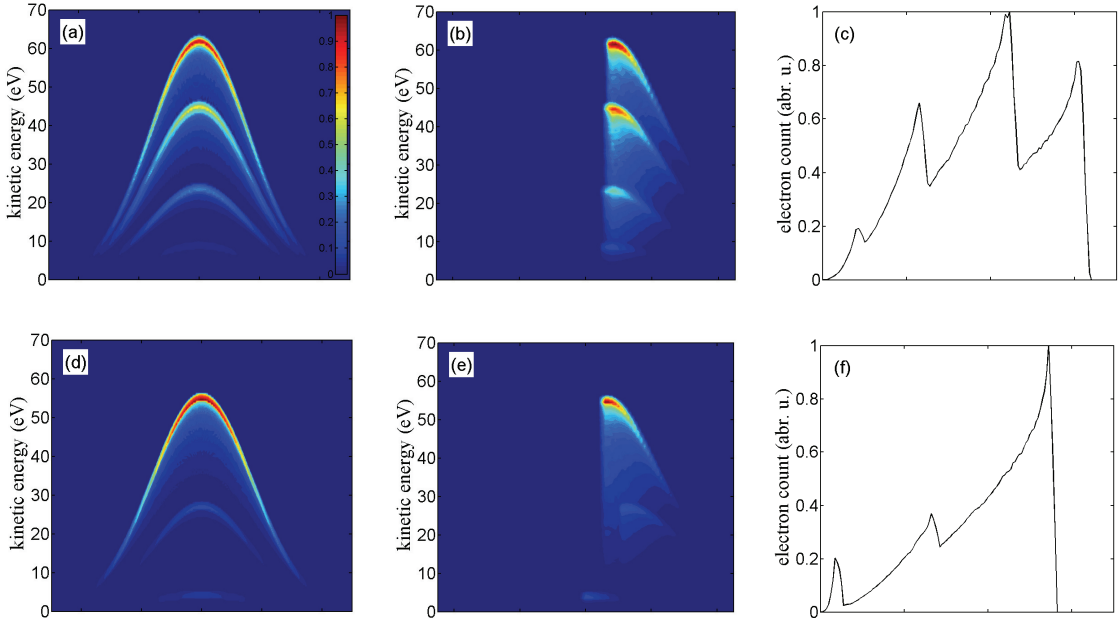
2.2 Highly directional, monoenergetic electron beams with few-cycle pulses

We present several emission maps to reveal the fine structure of the acceleration process and to arrive to conclusions about the macroscopically observable parameters of the generated electron beams. We examined the final kinetic energy distribution of the plasmon-accelerated electrons along the plasmon propagation direction (x-axis representing emission locations along the surface) for a few-cycle interacting pulse with a Gaussian pulse shape, 15 fs and 5 fs intensity FWHM, $\varphi_0 = 0$ carrier-envelope phase (with envelope and field maxima coinciding) and 800 nm central wavelength. The pulse was assumed to be focussed to a spot with a diameter of 4 μm on the prism surface reaching a peak plasmon field strength of 5.8×10^8 V/cm (Keldysh-gamma of 0.31). With this intensity value we have already taken into account that substantial field enhancement factors (up to $\times 100$) can be achieved with respect to the plasmon generating field. The inherent field enhancement in plasmonic fields secures both that the tunnelling emission regime is reached even for modest pulse energies and that highly efficient electron acceleration up to keV energies can take place as observed experimentally^{12,18,19}.

With these simulation parameters we calculated the spatial and spectral distribution of the emitted electrons along the plasmon propagation direction (in false colour representation in Figs. 3 a), d)) for two different pulse lengths to illustrate few-cycle effects. Whereas in the multi-cycle regime (15 fs pulse length) in Fig. 3 a) a much more structured distribution can be observed, in Fig. 3 d) (5 fs pulse length) the emission is mostly concentrated in a single structure on the emission map providing a better-behaved electron beam. We can also see that the emission of high-energy electrons is localized to the centre of the illuminated spot and that the number of distinct structures on the emission maps roughly correspond to the number of optical cycles in the generating pulse.

There is an even more conspicuous property that seems crucially important from the point-of-view of the applications of this electron source. Figs. 3 b) and e) depict the angular – kinetic energy distributions of the emitted electron beams showing in which direction the energetic electrons leave the surface. We can see that the emission is confined to a small range of angles supporting a directionally emitted electron beam ideally suited for novel ultrafast techniques. Provided that the pulse length is in the few-cycle-range (Fig. 3 e)) the angular emission map is reduced to a single distinct structure corresponding to a highly directional, quasi-monoenergetic electron beam representing the most favourable case of SP enhanced electron acceleration. By integrating any of the distributions along the x -axis we end up with the macroscopically observable electron spectra depicted in Fig. 3 c) and f). The spectrum in Fig. 3 f) has a $\Delta E/E$ value of 0.22 corresponding to a quasi-monoenergetic spectrum (E denotes the electron kinetic energy here). Under experimental circumstances the spectral properties of this electron beam can be further enhanced by applying a retarding potential to suppress the low-energy wing of the spectrum.

The fact that the appearance of high energy electrons is confined to the central portion of the surface, prompted us to investigate what happens to the angular distribution if one confines the emission on the prism surface to a limited, nanoscopic range. This is illustrated in Figs. 3 g) – 3 i) where the same emission maps and spectra are given as in Figs. 3 d) – 2 f) with the only difference that electrons coming only from a 300 nm wide strip of the surface were considered. It is possible to realize such a situation with experimental nanofabrication tools, for example, by depositing a dielectric layer on top of the metal coated prism which has a narrow opening to let electrons escape. By confining the emission area this way it can be seen that the distribution in Fig. 3 h) shows a highly enhanced contrast. This means that even more monoenergetic spectra and even more directional beams can be generated from this spatially confined source. This way the $\Delta E/E$ value on the integrated spectrum can be enhanced by almost an order of magnitude to 0.033, as depicted in Fig. 3 i). Thereby our results suggest that SP electron acceleration offers a robust and powerful technique for the generation of ultrafast, monoenergetic, highly directional electron beams.



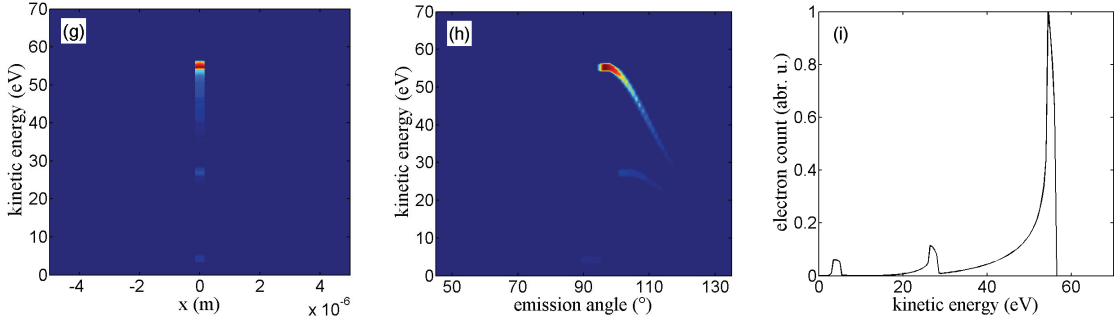


Fig. 3. Normalized photoacceleration maps (the kinetic energy distribution of electrons emitted at different points of the surface, a), c) and g), in false colour representation), angular and kinetic energy distribution (b), d) and h)) and macroscopic electron spectra (e), f) and i)) of surface plasmon accelerated electrons for three emission ranges: (a)-(c)) for 15 fs, (d)-i)) for 5 fs laser pulses with 800 nm central wavelength. In g)-i) we considered emission only from the depicted 300 nm wide region illustrated in g). This corresponds to a nanolocalized emission region achievable with nanofabrication techniques.

2.3 The role of the carrier-envelope phase

It is known that the carrier-envelope phase of few-cycle pulses has a measurable effect on laser-solid interaction processes even in the perturbative regime of nonlinear optics²⁻⁵. Motivated by these findings we also examined the effect of the optical waveform on the electron beam generated in this parameter regime. The angle-energy distributions in Figs. 4 a) and 4 b) (carrier-envelope phases of $\pi/2$ and π , respectively) can be directly compared to that of Fig. 3 e) (carrier-envelope phase $\varphi_0 = 0$); the only difference in the input parameters is that we varied the carrier-envelope phase of the interacting pulses but otherwise left other parameters unchanged.

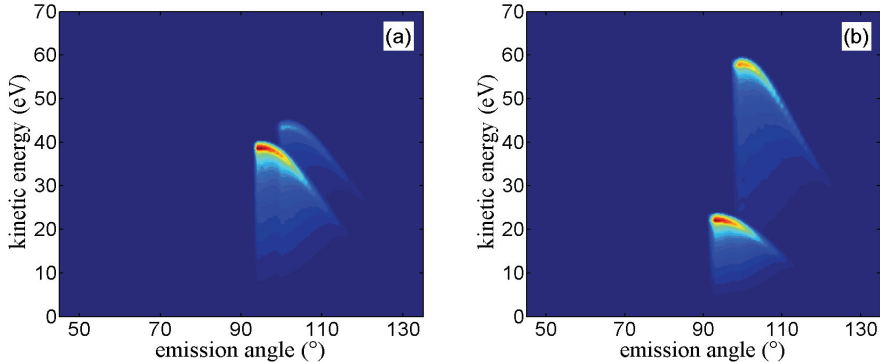


Fig. 4. Normalized photoacceleration maps (the kinetic energy distribution of electrons emitted at different angles from the surface) in false colour representation for two different carrier-envelope phase values ($\varphi_0 = \pi/2$ for a) and $\varphi_0 = \pi$ for b)) The laser pulse length was 5 fs, intensity FWHM.

We can see that the spectral cut-offs determined by the acceleration process are highly dependent on the carrier-envelope phase of the pulses in accordance with previous results²⁰. In our case, however, by having taken tunnelling emission into account (instead of multiphoton emission) the influence of the CE phase becomes more pronounced. The number of structures observable on the emission maps (and the integrated spectra – see accompanying animation) correspond to the number of optical cycles in the laser pulse (2 in this case). However, for carrier-envelope phase values between 1.75π and $\pi/4$ these structures coincide serving as a basis for an ideal photoelectron source. Therefore the generation of electron beams with the desired features requires state-of-the-art laser sources with phase stabilization.

4. FOCUSING CARRIER-ENVELOPE PHASE-STABILIZED PULSES ON SURFACES

Interaction of few-cycle pulses with surfaces poses more complex questions in terms of diffraction phenomena than laser-atom interactions. In most experimental schemes the surface is placed at a non-normal incidence angle into a focussed beam. In case of photoemission experiments the incidence is close to grazing^{2,3}. Whereas in surface plasmonic schemes the coupling angle of SPs determines it, which is close to 45 degrees. This means that one has to investigate the effective carrier-envelope phase value at each point of the surface and establish whether any spatial smearing effect could reduce the CE phase sensitivity of the process. In this section I present an estimation on the magnitude of this effect.

To this end analytic formulae from Ref. 24 were used to evaluate phase shifting effects in the focal vicinity of focussed Gaussian beams. The approximation enables us to take into account all relevant effects concerning pulsed, focused Gaussian beams, such as the Gouy phase shift in the focus and also the phases of off-axis points. After determining relative phase shift value at each point of the focal volume we could evaluate the influence of the nonuniformity of the CE phase value across the illuminated metal surface. For this, we assumed that a 3-photon process takes place (as a result of which, for example, electrons are emitted from the surface with a probability proportional to the third power of the beam intensity at a given point). From each point the number of the emitted electrons is also determined by the effective CE phase value “seen” by that point, not just the intensity. In this case the local electron signal can be described as $Q(x,y,\varphi) = I(x,y)^3(M\sin(\varphi_0 + \varphi(x,y)) + 1)$ where x and y are Cartesian coordinates in the surface plane, I describes the intensity distribution on the surface, M is the contrast of the CE phase sensitivity of the phenomenon examined, φ_0 is a CE phase offset, $\varphi(x,y)$ is the distribution of the extra phase shift along the surface (occurring due to focusing). This latter quantity is depicted in Fig. 5 a) and b) for two cases. a) illustrates the CE phase shift on a surface illuminated under grazing incidence (85°) without the presence of a dispersive medium. This example corresponds to our previous experiment with multi-photon induced photoemission. b) describes a case closely related to SP enhanced electron acceleration setups where focussing takes place through a dispersive medium under close to 45° angle of incidence to achieve SP coupling. In this case the phase pattern observed in a) are smeared by the dispersive phase shifting effect of the medium itself. By integrating the above expression in 2D across the illuminated surface in the vicinity of the focus we arrive to estimates for the reduction of the CE phase contrast in both types of experiments. This is illustrated in Fig. 5 c) for different angles of incidences.

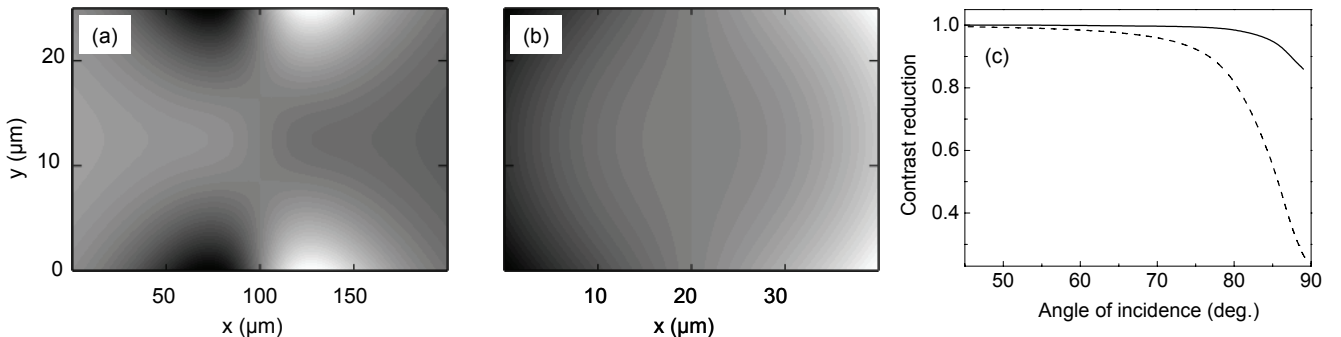


Fig 5. Illustration of phase shift in a focused beam along a surface illuminated with a beam impinging at different, non-normal angles of incidence. a) is for an incidence angle close to grazing (85°) and the beam propagates in vacuum. b) is for a beam propagating in fused silica corresponding to the SP coupling geometry in SP enhanced electron acceleration. The angle of incidence is 45° . The full greyscale in a) corresponds to a phase difference of 2.8π , whereas in b) for 6.2π . c) depicts the reduction of the visibility of the carrier-envelope phase-sensitivity if a surface-integrated signal is measured. The original M modulation depth (with respect to the CE phase) is reduced to M_s in the surface integrated signal. The contrast reduction is defined as M_s/M .

We can see that the closer one gets to grazing incidence the higher contrast deterioration can be expected. As expected, the effect can be much more severe in a dispersive medium. However, parameter regimes can still be found where spatial smearing effects do not affect significantly the CE phase contrast in a laser-surface interaction experiment. This is due to the intensity dependence of the signal: provided that most of the signal comes from the centre of the illuminated region, extreme CE phase smearing can be avoided since only a small portion of the electrons come from areas with high phase modulation (like the top and bottom stripes in Fig. 5 a)). Further investigations are also under way to establish similar effects in out-of-focus planes and for the case of tunnelling electron emission.

5. SUMMARY

Controlled optical waveforms and CE phase stabilized laser pulses are key tools to understand and to govern electronic transitions in solids. The continuous development of experimental techniques will enable researchers to perform true coherent control in these experimental schemes, too, where (as opposed to most femtochemistry techniques) the usage of few-cycle pulses is of high importance. To establish full coherent control, experimental techniques are required where not just carrier-envelope phase control is used but also pulse shaping is implemented in the few-cycle regime. With these tools combined with electron spectroscopic techniques one will be able to gain deeper understanding of the underlying ultrafast dynamics in solids. The proposed scheme of surface plasmon enhanced electron acceleration is an ideal candidate for extracting this information; moreover, this phenomenon can serve as a basis for a compact, direct carrier-envelope phase detector desired by the operators of attosecond beamlines. In addition, it has the potential to be used as a highly controllable electron source for ultrafast, high spatial resolution material characterization methods such as ultrafast electron diffraction and microscopy.

ACKNOWLEDGEMENTS

Support from the Hungarian Scientific Research Fund (OTKA Project F60256) is acknowledged. P. D. was also supported by the Bolyai Fellowship of the Hungarian Academy of Sciences.

REFERENCES

1. Agostini, P. and DiMauro, L. F., "The physics of attosecond light pulses" *Rep. Prog. Phys.* **67**, 813-855 (2004) and references therein.
2. Dombi, P., Apolonski, A., Lemell, C., Paulus, G. G., Kakehata M., Holzwarth, R., Udem, T., Torizuka, K., Burgdörfer, J., Hänsch, T. W., and Krausz, F., "Direct measurement and analysis of the carrier-envelope phase in light pulses approaching the single-cycle regime" , *New J. Phys.* **6**, 39 (2004)
3. Apolonski, A., Dombi, P., Lemell, C., Paulus, G. G., Kakehata M., Holzwarth, R., Udem, T., Torizuka, K., Burgdörfer, J., Hänsch, T. W., and Krausz, F., "Observation of light-phase-sensitive photoemission from a metal" , *Phys. Rev. Lett.* **92**, 073902 (2004)
4. Fortier, T. M., Roos, P. A., Jones, D.J., Cundiff, S. T., Bhat, R. D. R. , Sipe, J.E., "Carrier-envelope Phase-controlled Quantum Interference of Injected Photocurrents in Semiconductors" , *Phys. Rev. Lett.* **92**, 147403 (2004)
5. Mücke, O. D., Tritschler, T. , Wegener, M. , Morgner, U., Kärtner, F. X., Khitrova, G., Gibbs, H. M., "Carrier-wave Rabi flopping: role of the carrier-envelope phase" *Opt. Lett.* **29**, 2160-2162 (2004).
6. Aeschlimann M., et al., "Adaptive subwavelength control of nano-optical fields" *Nature* **446**, 301-304 (2007).
7. Stockman, M., Kling, M. F., Krausz F., and Kleineberg, U., "Attosecond nanoplasmnic field microscope" *Nature Photon.* **1**, 539-544 (2007).
8. Lobastov, V. A., Srinivasan R., and Zewail, A. H. , "Four-dimensional ultrafast electron microscopy" *Proc. Nat. Acad. Sci.* **102**, 7069-7073 (2005).
9. Siwick, B. J., Dwyer, J. R., Jordan, R. E., and Miller, R. J. D. , "An atomic-level view of melting using femtosecond electron diffraction" *Science* **302**, 1382-1385 (2003).

10. Hommelhoff, P., Kealhofer, C., Kasevich, M. A., "Ultrafast Electron Pulses from a Tungsten Tip Triggered by Low-Power Femtosecond Laser Pulses" Phys. Rev. Lett. **97**, 247402 (2006).
11. Ropers, C., Solli, D. R., Schulz, C. P., Lienau C. and Elsaesser, T., "Localized Multiphoton Emission of Femtosecond Electron Pulses from Metal Nanotips" Phys. Rev. Lett. **98**, 043907 (2007).
12. Irvine, S. E. , Dechant, A. , Elezzabi, A. Y., "Generation of 0.4-keV Femtosecond Electron Pulses using Impulsively Excited Surface Plasmons" Phys. Rev. Lett. **93**, 184801 (2004).
13. Jones, D. J. , Diddams, S. A. , Ranka, J. K. , Stentz, A. , Windeler, R. S. , Hall, J. L., and Cundiff, S. T. , "Carrier-Envelope Phase Control of Femtosecond Mode-Locked Lasers and Direct Optical Frequency Synthesis," Science **288**, 635-639 (2000).
14. Yakovlev, V. S., Dombi, P., Tempea, G. , Lemell, C. , Burgdörfer, J. , Udem, T., and Apolonski, A., "Phase-stabilized 4-fs pulses at the full oscillator repetition rate for a photoemission experiment" Appl. Phys. B **76**, 329-332 (2003).
15. Lemell, C., Tong, X.-M., Krausz, F., and Burgdörfer, J., "Electron Emission from Metal Surfaces by Ultrashort Pulses: Determination of the Carrier-Envelope Phase," Phys. Rev. Lett. **90**, 076403 (2003).
16. Dombi, P., Krausz, F., Farkas, G., „Ultrafast dynamics and carrier-envelope phase sensitivity of multiphoton photoemission from metal surfaces”, J.Mod. Opt. **53**, 163-172 (2006).
17. Georges, A. T., private communication.
18. Zawadzka, J., Jaroszynski, D., Carey, J. J., and Wynne, K., "Evanescent-wave acceleration of ultrashort electron pulses" Appl. Phys. Lett. **79**, 2130-2132 (2001).
19. Kupersztych, J., Monchicourt P., and Raynaud, M., "Ponderomotive Acceleration of Photoelectrons in Surface-Plasmon-Assisted Multiphoton Photoelectric Emission" Phys. Rev. Lett. **86**, 5180-5183 (2001).
20. Irvine, S. E., Dombi, P., Farkas, G. and Elezzabi, A. Y., "Influence of the Carrier-envelope Phase of Few-cycle Pulses on Ponderomotive Surface-plasmon Electron Acceleration" Phys. Rev. Lett. **97**, 146801 (2006).
21. Corkum, P. B., "Plasma perspective on strong-field multiphoton ionization" Phys. Rev. Lett. **71**, 1994-1997 (1993).
22. Raether, H., *Surface plasmons on Smooth and Rough Surfaces and on Gratings* (Springler-Verlag 1988)
23. Irvine, S. E., Elezzabi, A. Y., "Surface-plasmon-based electron acceleration", Phys. Rev. A **73**, 013815 (2006).
24. Porras, M. A., "Diffraction effects in few-cycle optical pulses", Phys. Rev. E **65**, 026606 (2002).